# Effect of A-tract-mediated linker histone orientation on trinucleosome compaction

Madhura De[1,2,3], Martin Würtz[1,4], Gabriele Müller[1,6], Katalin Tóth[1,7*], Rebecca C. Wade[2,3,4,5*]

[1]Division of Biophysics of Macromolecules, German Cancer Research Center (DKFZ), 69120 Heidelberg, Germany
[2] Molecular and Cellular Modelling Group, Heidelberg Institute for Theoretical Studies (HITS), 69118 Heidelberg, Germany
[3] Faculty of Biosciences, Heidelberg University, 69120 Heidelberg, Germany
[4]Center for Molecular Biology (ZMBH), DKFZ-ZMBH Alliance, Heidelberg University, 69120 Heidelberg, Germany
[5]Interdisciplinary Center for Scientific Computing (IWR), Heidelberg University, 69120 Heidelberg, Germany
[6] Division of Brain Tumour Translational Targets, German Cancer Research Center (DKFZ), 69120, Heidelberg, Germany
[7] Present address: Department of Biophysics and Cell Biology, Faculty of Medicine, University of Debrecen, Hungary

*To whom correspondence should be addressed. Emails: Katalin Tóth: dr.toth.katalin@med.unideb.hu, Rebecca C. Wade: rebecca.wade@h-its.org

## Abstract

Linker histones (LH) have been shown to preferentially bind to AT-rich DNA, and specifically to A-tracts, contiguous stretches of adenines. Recently, using spFRET (single pair Förster/Fluorescence Resonance Energy Transfer), we showed that the globular domain (gH) of *Xenopus laevis* H1.0b LH orients towards A-tracts present on the linker-DNA (L-DNA) in LH:mononucleosome complexes. We investigated the impact of this A-tract mediated orientation of the gH on the compaction of higher-order structures by studying trinucleosomes as minimal models for chromatin. Two 600 bp DNA sequences were constructed containing three Widom 601 core sequences separated by about 40 bp linkers and A-tracts inserted on either the outer or the inner L-DNAs flanking the 1st and the 3rd Widom 601 sequences. The two inner L-DNAs were fluorescently labelled at their midpoints. Trinucleosomes were reconstituted using the doubly-labelled 600 bp DNA, core histone octamers and the full-length H1.0b LH. SpFRET was performed for a range of NaCl concentrations. While the LH compacted the trinucleosomes, surprisingly, the extent of compaction was similar for trinucleosomes with A-tracts either on the two outer or on the two inner L-DNAs. Modeling constrained by the FRET efficiency suggests that the trinucleosomes adopt a zig-zagged conformation with the 1st and 3rd nucleosomes stacked on top of each other. Even though we expect that the gH of neighbouring (1st and 3rd) LHs are oriented towards the A-tracts, our models suggest that they are not sufficiently close to dimerize and affect compaction. Thus, despite differences in A-tract placements, the LH compacts trinucleosomes similarly.

## Highlights

1. Does the A-tract-mediated orientation of the LH gH affect chromatin structure?
2. Trinucleosomes with A-tracts on the outer or inner L-DNAs of nucleosomes 1 and 3 were reconstituted
3. spFRET-based modeling shows LH compacts trinucleosomes to a zig-zag conformation
4. The A-tract placement does not affect compaction of the LH-bound trinucleosomes.

**Keywords:** trinucleosomes, linker histone, single-pair FRET, A-tracts, AFM, chromatin structure

**Abbreviations:** NRL: Nucleosome Repeat Length, NCP: Nucleosomal core particle, spFRET: single pair Förster/Fluorescence Resonance Energy Transfer, L-DNA: linker DNA, LH: Linker histone, gH: globular (Head) domain of the LH, CTD: C-terminal domain of the LH, NTD: N-terminal domain of the LH, AFM: Atomic Force Microscopy

## Introduction

The highly positively charged linker histone (LH) H1 associates with the nucleosome in the region bounded by the linker-DNA (L-DNA) arms entering and exiting the nucleosome core particle (NCP) [1–5]. The LH has a tripartite structure composed of a conserved globular domain (gH), a 100 residue long, intrinsically disordered C-terminal domain (CTD) and a shorter N-terminal domain [6]. The gH has been observed to associate either in an on-dyad [2–5] or in an off-dyad [7,8] fashion. The positioning of the gH has been suggested, from both experimental [7,9] and computational studies [10], to affect the compaction of nucleosomal arrays.
The CTD has been observed to associate with one [4,7] or both L-DNA arms [5] experimentally, and in a salt-dependent manner with one (low salt) or both (high salt) L-DNAs, in coarse-grained simulations [11]. The association of the CTD with the L-DNAs has also been suggested to have an effect on the charge distributions of nucleosomal arrays [4]. How would the gH or the CTD affect compaction of a nucleosomal array? In order to address this question, the gH of LHs of neighbouring nucleosomes could be made to associate with the nucleosomes in a specific manner, either by mutating the gH domain residues that determine on- or off-dyad binding [8], or by exploiting the preference of the LH gH for AT-rich DNA or A-tracts (a series of contiguous adenines) [5,12–23].
In this study, we built on our observations by spFRET of mononucleosome-LH complexes [22] that showed that the gH domain of a full-length LH recognizes an 11 bp A-tract on the L-DNA and in order to mediate interactions with its minor groove, is oriented in a specific way (Figure 1B ii). We ask the question whether such A-tract mediated orientation of the gH domain affects the compaction of nucleosomal arrays. To address this question, we constructed trinucleosomes consisting of 600 bp DNA with three strongly nucleosome positioning Widom 601 sequences [24] situated about 40 bp apart from each other, thereby resulting in a nucleosome repeat length (NRL) of 187 bp. The flank sequences of nucleosomes (Nuc) 1 and 3 were either A-tract (11 contiguous adenines complementary to thymines) or purely GC-tract. Depending upon the location of the A-tracts (Table 1), the trinucleosome constructs were named A-far (A-tracts on outer L-DNA and GC-tracts on inner

L-DNA) or A-near (A-tracts on inner L-DNA and GC-tracts on outer L-DNA). Both the constructs were doubly labelled at the mid-points of the two inner L-DNAs with the fluorophores Alexa 488 and Alexa 594 (Figure 1A).

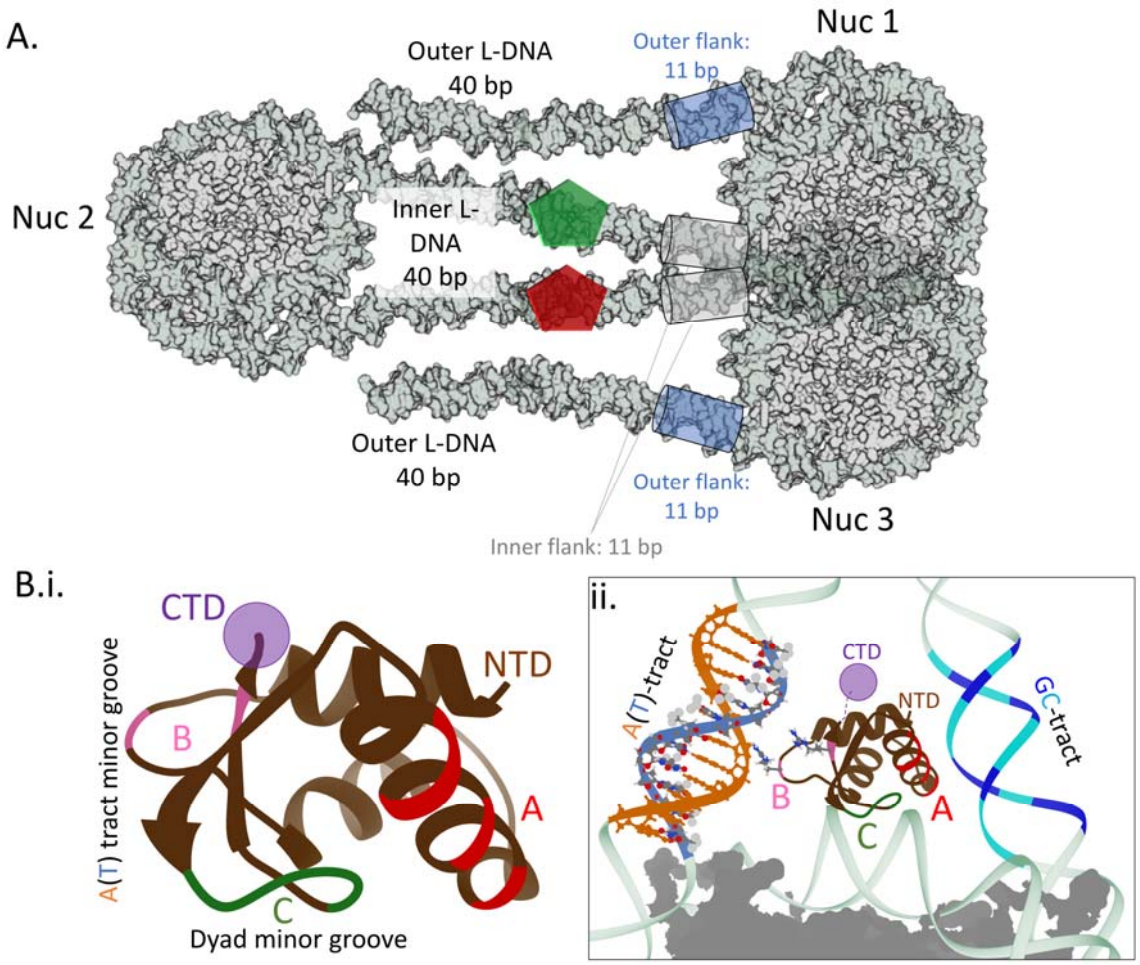


**Figure 1: A.** Schematic illustration of the trinucleosome systems studied. The three nucleosomes, Nuc 1, 2, and 3 are shown with the outer and inner L-DNAs labelled. The LH is not shown. The the outer (blue) and inner (grey) flanks of the L-DNA arms are shown by cylinders. Fluorophores attached to the mid-points of the inner L-DNAs are represented by green (Alexa 488 or donor) and red (Alexa 594 or acceptor) pentagons. **B. (i)** Cartoon representation of the globular domain (gH) of the LH (PDB ID 5NL0 [4]) showing three DNA interacting zones, A, B and C [22]. Zone B can interact with and mediate recognition of A-tracts. The start of the C-terminal domain (CTD) is represented by a purple circle. **(ii)** Binding of the LH gH to a nucleosome with an A-tract flank on one of the L-DNA arms. The on-dyad gH is oriented towards the A-tract (dA in orange, dT in blue) minor groove on the L-DNA, with interactions mediated by arginines in zone B [22]. The gHs that bind to Nuc 1 and Nuc 3 in the trinucleosome constructs are expected to be similarly oriented to the A-tract flanking sequences.

**Table 1: Flank sequences of the outer and inner L-DNA arms for the A-near and A-far trinucleosomes**

| Trinucleosome construct | Inner L-DNA flank sequence | Outer L-DNA flank sequence |
|---|---|---|
| A-near | 5′- AAAAAAAAAAA -3′<br>3′- TTTTTTTTTTT -5′ | 5′– GGGCGGCCGCG –3′<br>3′- CCCGCCGGCGC –5′ |
| A-far | 5′– GGGCGGCCGCG –3′<br>3′- CCCGCCGGCGC –5′ | 5′- AAAAAAAAAAA -3′<br>3′- TTTTTTTTTTT -5′ |

To ensure that the three DNA fragments, corresponding to each of the three nucleosomes, in the 600 bp construct were correctly oriented with respect to each other, a modified Golden-Gate assembly [25–27] was performed *in vitro* (see Supplementary Information section 1). In this method, the use of a Type IIs restriction enzyme (BsaI-HF-v2, purchased from New England Biolabs) that produces unique 4 bp sticky ends, ensures that the three fragments are oriented in a single way. After gel extraction and purification of the 600 bp DNA sequences, A-far and A-near, reconstitution of the trinucleosomes was performed as described in Supplementary Information section 2 and in our earlier work [22]. Four types of trinucleosomes were reconstituted from the 600 bp DNA doubly-labelled with fluorophores, full-length wild-type *Xenopus laevis* core histone octamers (Planet Protein, Colorado), and full length wild-type, *X. laevis* LH of subtype H1.0b that was purified using the protocol described previously [22]. The trinucleosome constructs were A-near with and without LH and A-far with and without LH. Reconstitution was checked using 1% agarose gel electrophoresis and atomic force microscopy (AFM) as described in Supplementary Information section 2 and in reference [28].
Measurements for the four types of were carried out using single-laser excitation (with 491 nm, Cobolt Calypso, Hübner Photonics, Germany) spFRET (single-pair Förster/Fluorescence Resonance Energy Transfer) as described previously [29,30]. From spFRET measurements we obtained the proximity ratio, which is directly proportional to the FRET efficiency. The proximity ratio is calculated by dividing the number of photons detected in the acceptor channel ($N_A$) by the total number of photons detected in the acceptor and donor ($N_D$) channels, i.e. $P = N_A/(N_A+N_D)$ [31–33].
Models of the trinucleosomes with the gH were built using the softwares Chimera [34] and FRET Positioning and Screening (FPS) [35,36]. We observed that despite the A-tract mediated orientation of the gH domain, there was no difference in the compaction of the two trinucleosomes containing A-tracts in different locations.

## The linker histone H1.0b compacts trinucleosomes similarly irrespective of the placement of A-tract flanking sequences

SpFRET [22,29,31,31–33,37,38] was performed on the trinucleosomes under NaCl concentrations of 25, 75, 150, 250, 300, 550 and 700 mM NaCl, with 10 mM Tris and0.1 mM EDTA (ethylene diamine tetraacetic acid) at pH 7.5. This was done to observe how the trinucleosomes dissociation with an increase in salt concentration, and how the presence of the LH affects such dissociation [39–41].
Proximity ratio histograms from all replicates and graph fittings are given in Supplementary Information section 3B (Figures S4 to S10). The proximity ratio histograms obtained from a single replicate for each of the four trinucleosome systems for the seven salt concentrations are shown as heatmaps in figure 2A. For both the trinucleosomes with LH (Figure Ai and ii), the proximity ratios of the major population peak(s) are higher than the major population peak of the trinucleosome without LH (Figure 1.Aiii), at salt concentrations from 25 mM to 250 mM. This difference suggests that the LH compacts the trinucleosomes, bringing the inner L-DNA arms closer to each other. Shielding of the negative charges on the DNA backbone by the positively charged sodium ions also brings the two inner L-DNA arms closer to each other in trinucleosomes lacking LH (Figure 1Aiii). This increase in compaction as a result of charge shielding by the salt is more prominent in trinucleosomes lacking LH than trinucleosomes associated with LHs (Figure 2B i-iv, 25 mM vs. 150 mM NaCl).

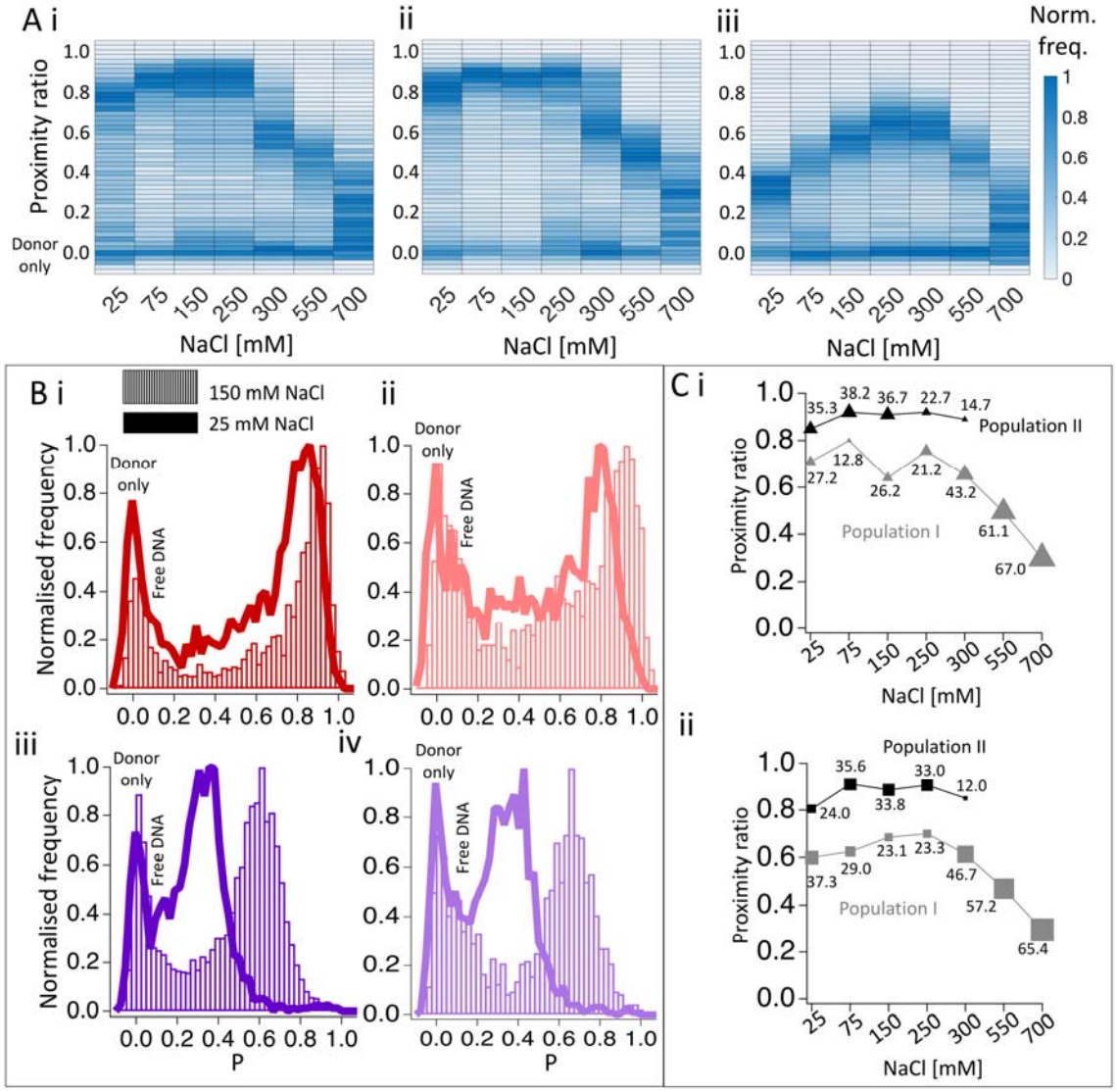


**Figure 2: A.** Heat-map representations of proximity ratio histograms measured by spFRET under NaCl concentrations ranging from 25 to 700 mM for the trinucleosome systems. **(i)** A-near with LH, **(ii)** A-far with LH, and **(iii)** A-near without LH. The proximity ratio histograms were similar for A-far without LH to those for A-near without LH (see Supplementary Information Section 3BI).. The y-axis represents proximity ratio, the x-axis NaCl concentrations (25 to 700 mM). The colour intensity represents the normalised frequency of the proximity ratio value. **B.** Proximity ratio (P) histograms for 25 mM (solid line) and 150 mM (bars) of NaCl for A-far with LH **(i)**, A-near with LH **(ii)**, A-near without LH **(iii)** and A-far without LH **(iv)**. **C.** Plots of mean proximity ratio (y-axis) of populations I and II of the high proximity ratio major population peak (see Supplementary Information section 3B.I. 1-7) against salt (x-axis). The marker size and label show the % population of the peak.). **(i)** A-near with LH, **(ii)** A-far with LH. For A-near without LH, see Supplementary Information 3B. II, Figure S11).

However, we observe that the LH compacts the A-near and A-far trinucleosomes similarly. Upon fitting the plots to multiple Gaussians, using Matlab (see Supplementary Information section 3B), we observe that the high proximity ratio major population peak can be deconvoluted into two species in trinucleosomes containing the LH. These are referred to as Population I (the lower mean proximity ratio of the two) and Population II (the higher mean proximity ratio). Figure 2C shows the populations of the mean proximity ratios of A-near

with LH (Figure 2C i) and A-far with LH (Figure 2C ii). Population II maintains a consistent mean proximity ratio of ca. 0.85, while the mean proximity ratio of population I varies between 0.6 and 0.7 at a salt range of 25 to 250 mM. These two populations both exist between salt concentrations of 25 and 250 mM. At 300 mM salt concentration, population II disappears (Supplementary Information Section 3B I. 5.), possibly due to dissociation of the LH. From salt concentrations of 300 to 700 mM, the mean proximity ratio of population I (300 mM) or the major population (550 and 700 mM) of trinucleosomes with LH becomes similar to trinucleosomes without LH, indicating dissociation of LH. Using a proximity ratio value of 0.8, we next modelled population II of the trinucleosomes with LH.

## Trinucleosomes modeled using measured proximity ratio values have a 2-start helical arrangement

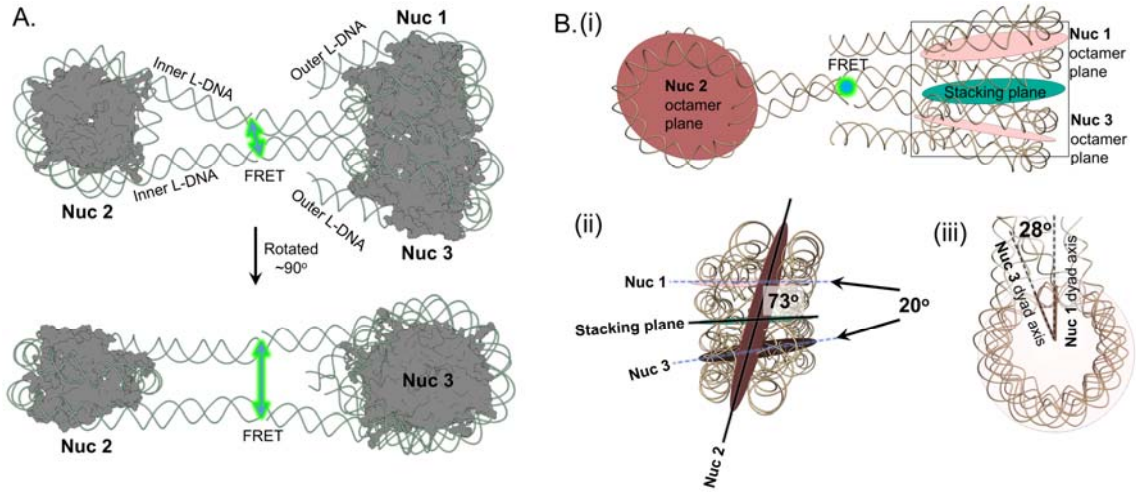


**Figure 3: A.** Two perpendicular views of a model of a trinucleosome with a computed proximity ratio between the labels on the inner L-DNA arms of 0.8 (representative of Population II). The outer L-DNAs are truncated for clarity. The green arrows represent energy transfer between the fluorophore labels (which are not shown). Nuc 1 and nuc 3 stack. **Bi - iii.** Geometric parameters defining the structure of the model computed using Chimera [34]. **(i)** Three octamer planes shown in pink with thestacking plane between Nuc 1 and Nuc 3 shown in green. **(ii)** The angle between the stacking plane and Nuc 2 is 73° and between the octamer planes of Nuc 1 and Nuc 3 is 20°. **(iii)** The angle between the dyad axes of Nuc 1 and Nuc 3 is 28°.

In order to model the trinucleosomes, the experimentally determined starting structure of the mononucleosome-linker histone complex, PDB 5NL0 [4], was mutated to the sequence of Nuc 2 using Chimera [34]. This structure of Nuc 2 was then subjected to elastic network normal mode analysis using the elNémo webserver [42]. This enabled us to obtain a range of arm-opening conformations [20–22]. To the ensemble thus generated, accessible volume simulated fluorophores were attached on the labelling positions (at the methyl group of the thymine residue at the mid-point of each inner L-DNA arm), using the software FPS [35,36], with dye parameters described in references [22,35,36,43]. The model that showed a computed FRET efficiency proximity ratio of 0.8 was selected. To this structure of Nuc 2, two more copies of the PDB structure (PDB 5NL0) were added, and the resulting DNA was renumbered and mutated to that of the A-near and A-far sequences using the 'swapna' command of Chimera [34]. The gH domain was placed on Nuc 2 in a canonical on-dyad

fashion as observed in the structures with PDB identifiers: 4QLC [2], 5WCU [3], 5NL0 [4], and 7K5X [5]. The gH domains on Nuc 1 and Nuc 3 were positioned according to the AG and GA models described in our earlier work [22], i.e., on-dyad, with Zone B proximal to the A-tract minor groove.

While building the model, apart from the single spFRET restraint, we also ensured that the L-DNAs were not kinked or bent at an angle. Thus, by keeping the inner L-DNAs straight, we see that the Nuc 1 and 3 stack on top of each other (Figure 3A), resembling the canonical 2-start helical arrangement [44] as predicted and observed for 187 NRL nucleosomes [45–47]. The stacking is optimal and was checked by aligning it to PDBs 6HKT [46] and 6L49 [48]. Chimera [34] was used to obtain structural parameters. Figure 3B i shows the green stacking plane between Nuc 1 and 3 that was defined by selecting the residues on the core histone octamer that faced each other: from H3 histone of Nuc 1 and 3, Arg 134, from H4, Asp 24, from H2A, Asn 68, and from H2B, Ser 120. This stacking plane was used to calculate the screw angle between the Nuc 2 and the stacked Nuc 1 and 3, which was found to be 73° (Figure 3B ii). The dyad axis of Nuc 1 and 3 were defined on each nucleosome by the two dyad bases and Arg 134 of two H3 copies. These axes were rotated by 28° with respect to each other.

To understand why despite placing A-tracts on the outer or inner L-DNA arms, the two types of trinucleosomes were compacted similarly by the LH, we focus on the gH associations on Nuc 1 and Nuc 3.

## The orientation of neighbouring linker histones does not influence trinucleosome compaction

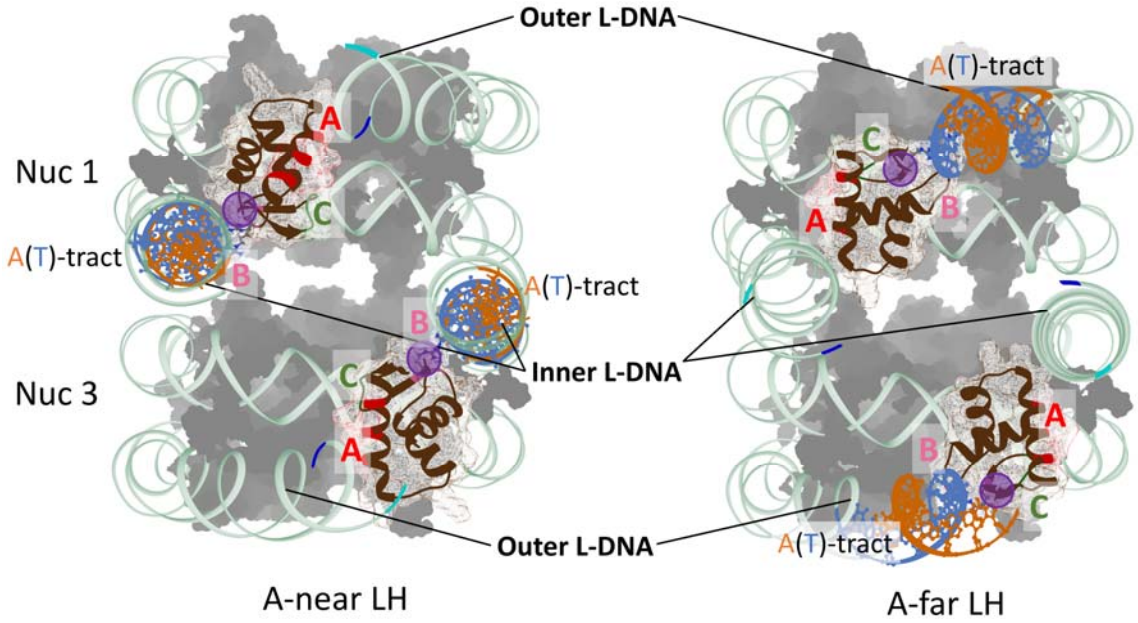


**Figure 4:** Stacking of LH-bound Nuc 1 and Nuc 3 . Left: A-near and Right: A-far with LH. Each LH is shown with its gH on-dyad and oriented towards the A-tracts [22]. The LH gH is represented by a brown ribbon and surface. The start of the CTD in the gH domain is represented by a purple circle. The three zones A, B and C are colour coded as in Figure 1. The core histone octamers are represented as grey surface, DNA in pale green.The adenines are in orange, thymines are in blue and in ball and stick representation. The tips of the L-DNA containing the GC-tract are coloured cyan and deep blue.

The location of the gH [7,8,10] and the CTD [4] has been suggested to play an important role in the formation of higher-order structures of chromatin. The gH can be associated either on- [2–5,8] or off-dyad [7,8,20]. Experimental [2,7] and computational [10] studies suggested that these different locations of the gH can affect the compaction of higher-order structures. It was also suggested that off-dyad positioned gH may be able to self-associate and hence affect the compaction of arrays [7]. The CTD was observed to associate with one L-DNA arm in cryo-EM structures [4], leading to suggestions that this asymmetric association of the LH can lead to different charge distributions in arrays [4].

Recently, we observed, using spFRET, and modeling based on spFRET-derived distances, that A-tracts placed on the L-DNA orient the on-dyad positioned gH such that two conserved arginines (R42 and R94) on the gH (Zone B) are proximal to the minor groove of the A-tract [22]. Do orientational differences of the gH affect the compaction of nucleosomal arrays? Using A-tracts to orient gH domains of neighbouring LH to face different directions, we observed that it did not change the way the trinucleosomes were compacted. We focus on the gH domains of Nuc 1 and 3 (Figure 4). Although we did not directly observed the location of the full-length LH in our trinucleosome experiments, we assume that the gH (of LH of subtype H1.0b) would be associated on-dyad [4,5,49] and its orientation would be similar to that that we observed for A-tract-containing mononucleosomes [22]. In A-near (Figure 4 left), the A-tracts are on the inner L-DNA and in A-far, they are on the outer L-DNA (Figure 4 right). The gH domains on Nuc 1 and Nuc 3, both associated on-dyad, are not close enough to each other to self-associate. This suggests that the orientation of the gH domains of the LH H1.0b does not play a role in the compaction of the trinucleosomes. But what about the CTD?
The purple circles in Figure 4 represent the C-terminus of the gH domain, corresponding to the start of the 100-residue long intrinsically disordered tail. If the CTDs associate with the L-DNA arm to which the C-terminus of the gH (purple circle) is close, then, for A-near (Figure 4 left), it would associate with the inner L-DNA arm and for A-far (Figure 4 right), with the outer L-DNA arm. In this case, we would expect that the highly positively charged CTD would compact A-near by bringing the inner L-DNAs closer together with respect to A-far. In our work with mononucleosomes, we have observed that position 101 (6 residues into the CTD) is nearly equidistant from both L-DNA arms [22]. Zhou *et al.* (2021) [5] observed that the CTD of LH H1.0b (PDB 7K5X) associates with both L-DNA arms. But coarse grained simulations have shown that the CTD can associate with one L-DNA at low salt (5 and 15 mM), and with both L-DNA arms at high salt (80 and 150 mM) concentrations [11]. If this is the case, then we would expect that A-near would be more compact in low salt concentrations compared to A-far. Figure 2C show that the mean proximity ratio peak of Population I of A-near with LH (Figure 2C i) is higher than A-far with LH (Figure 2C ii) at a salt concentration of 25 mM (difference between $P_{mean}$ of A-near and A-far with LH population I at 25 mM is about 0.1, Supplementary Information Section 3B), whereas the highly compact Population II shows similar mean proximity ratios ($\Delta P_{mean}$ at 25 mM is 0.05 for population II for 'with LH' trinucleosomes) in both trinucleosome types. We ignore Population II of A-near with LH at 75 mM salt (Figure 2C i), since the relative population is just 12%. Supplementary section 3B. part 1 (25 mM) suggest that both the reconstitution replicates show a higher proximity ratio of A-near with LH population I. This might reflect what was proposed by Luque *et al.* (2014) [11] that the CTD associates with one L-DNA at low salt. At 25 mM NaCl, if the CTD indeed associates with the inner L-DNA arms in A-near (Figure 4 left) then they might associate with

and bring the two inner L-DNA arms slightly closer in A-near than in A-far. However, overall, i.e. including both populations I and II, the mean proximity ratios of the two trinucleosomes are similar as the salt concentration is raised, suggesting that the CTD associates with both the arms and compacts both the trinucleosomes similarly, despite the location of A-tracts.

## Conclusion

We show that different locations of A-tracts, despite reorienting the LH gH domain [22], do not affect LH-mediated trinucleosome compaction. This could be because the LH subtype we use in our experiments, the H1.0b, has been observed to associate in an on-dyad fashion [4,5,49]. For the gH to affect compaction of a nucleosomal array, it would be expected to self-associate or form salt-bridges. In our case, the gH domains on Nuc 1 and Nuc 3 are not close enough for dimerization (Figure 4). We suggest that in on-dyad positioned LH, the compaction of nucleosomal arrays could be mediated by the CTD. Both the A-far and A-near trinucleosomes show the coexistence of two populations in the presence of LH, with the more compact one (population II) decreasing sharply at 300 mM NaCl. At a low salt concentration of 25 mM, both the populations of A-near with LH are slightly more compact than that of A-far with LH. This could be possible if at 25 mM NaCl, the CTD indeed associates with the L-DNA it is closer to (inner for A-near, Figure 4 left). At higher salt concentration, the proximity ratio of populations in A-near become similar to A-far, with LH. The presence of LH compacts the trinucleosomes (Figure 2). An increase in salt concentration indeed compacts trinucleosomes without LH (Figure 2Aiii), by charge shielding. This increase in compaction by charge shielding is higher for trinucleosomes without LH (Figure 2A Biii and iv), but the overall compaction remains more for trinucleosomes with LH at salt concentrations from 25 to 250 mM.
Our work shows that the preference for A-tracts by the LH can be exploited to study whether the orientation of the LH can affect nucleosomal arrays. Using LH of different isoforms and those that associate off-dyad can be used in a similar manner, in conjunction with differently located A-tracts, to study how the location of LH may affect higher-order compaction and structuring.

**Acknowledgements** The authors are very grateful to Prof. Jeffrey Hayes and Dr. Amber Cutter for providing us with the plasmid for wild type linker histone. The authors are grateful to Nathalie Schwarz for purifying the linker histone. This work was supported by the Helmholtz International Graduate School for Cancer Research (DKFZ) and the Klaus Tschira Foundation.

**Author contributions** MD, KT and RW conceived the research. MD, GM, KT designed the DNA constructs. MD and GM prepared and purified the DNA. MW acquired the AFM images. MD performed the spFRET measurements with suggestions from KT, and the modeling, with suggestions from RW, and wrote the paper with suggestions from all the authors. All the authors contributed to the finalisation of the manuscript.

**Data availability** Data is available in this repository:
https://doi.org/10.5281/zenodo.5090768. This repository includes the models of A-far and

A-near (.pdb) and raw data from the spFRET experiments (.t3r) in different salt concentrations, along with the donor-only and A-near DNA sample.

## References


[1] Y.-B. Zhou, S.E. Gerchman, V. Ramakrishnan, A. Travers, S. Muyldermans, Position and orientation of the globular domain of linker histone H5 on the nucleosome, Nature. 395 (1998) 402–405. https://doi.org/10.1038/26521.

[2] B.-R. Zhou, J. Jiang, H. Feng, R. Ghirlando, T.S. Xiao, Y. Bai, Structural Mechanisms of Nucleosome Recognition by Linker Histones., Mol Cell. 59 (2015) 628–638. https://doi.org/10.1016/j.molcel.2015.06.025.

[3] B.-R. Zhou, J. Jiang, R. Ghirlando, D. Norouzi, K.N. Sathish Yadav, H. Feng, R. Wang, P. Zhang, V. Zhurkin, Y. Bai, Revisit of Reconstituted 30-nm Nucleosome Arrays Reveals an Ensemble of Dynamic Structures, J Mol Biol. 430 (2018) 3093–3110. https://doi.org/10.1016/j.jmb.2018.06.020.

[4] J. Bednar, I. Garcia-Saez, R. Boopathi, A.R. Cutter, G. Papai, A. Reymer, S.H. Syed, I.N. Lone, O. Tonchev, C. Crucifix, H. Menoni, C. Papin, D.A. Skoufias, H. Kurumizaka, R. Lavery, A. Hamiche, J.J. Hayes, P. Schultz, D. Angelov, C. Petosa, S. Dimitrov, Structure and Dynamics of a 197 bp Nucleosome in Complex with Linker Histone H1., Mol Cell. 66 (2017) 384-397.e8. https://doi.org/10.1016/j.molcel.2017.04.012.

[5] B.-R. Zhou, H. Feng, S. Kale, T. Fox, H. Khant, N. de Val, R. Ghirlando, A.R. Panchenko, Y. Bai, Distinct Structures and Dynamics of Chromatosomes with Different Human Linker Histone Isoforms, Molecular Cell. 81 (2021) 166-182.e6. https://doi.org/10.1016/j.molcel.2020.10.038.

[6] P. Hohmann, Species- and cell-specific expression of H1 histones in tissue culture cells, Archives of Biochemistry and Biophysics. 205 (1980) 198–209. https://doi.org/10.1016/0003-9861(80)90099-5.

[7] F. Song, P. Chen, D. Sun, M. Wang, L. Dong, D. Liang, R.-M. Xu, P. Zhu, G. Li, Cryo-EM study of the chromatin fiber reveals a double helix twisted by tetranucleosomal units, Science. 344 (2014) 376–380. https://doi.org/10.1126/science.1251413.

[8] B.-R. Zhou, H. Feng, R. Ghirlando, S. Li, C.D. Schwieters, Y. Bai, A Small Number of Residues Can Determine if Linker Histones Are Bound On or Off Dyad in the Chromatosome, Journal of Molecular Biology. 428 (2016) 3948–3959. https://doi.org/10.1016/j.jmb.2016.08.016.

[9] B.-R. Zhou, J. Jiang, H. Feng, R. Ghirlando, T.S. Xiao, Y. Bai, Structural Mechanisms of Nucleosome Recognition by Linker Histones, Molecular Cell. 59 (2015) 628–638. https://doi.org/10.1016/j.molcel.2015.06.025.

[10] O. Perišić, S. Portillo-Ledesma, T. Schlick, Sensitive effect of linker histone binding mode and subtype on chromatin condensation, Nucleic Acids Research. 47 (2019) 4948–4957. https://doi.org/10.1093/nar/gkz234.

[11] A. Luque, R. Collepardo-Guevara, S. Grigoryev, T. Schlick, Dynamic condensation of linker histone C-terminal domain regulates chromatin structure, Nucleic Acids Res. 42 (2014) 7553–7560. https://doi.org/10.1093/nar/gku491.

[12] J. Zlatanova, J. Yaneva, Histone H1-DNA Interactions and Their Relation to Chromatin Structure and Function, DNA and Cell Biology. 10 (1991) 239–248. https://doi.org/10.1089/dna.1991.10.239.

[13] W. An, S.H. Leuba, K. van Holde, J. Zlatanova, Linker histone protects linker DNA on only one side of the core particle and in a sequence-dependent manner, Proc Natl Acad Sci USA. 95 (1998) 3396. https://doi.org/10.1073/pnas.95.7.3396.
[14] Käs, E., Izaurralde, E., & Laemmli, U. K., Specific inhibition of DNA Binding to nuclear scaffolds and histone H1 by distamycin., Journal of Molecular Biology. 210 (1989) 587–599. https://doi.org/10.1016/0022-2836(89)90134-4.
[15] K. Cao, N. Lailler, Y. Zhang, A. Kumar, K. Uppal, Z. Liu, E.K. Lee, H. Wu, M. Medrzycki, C. Pan, P.-Y. Ho, G.P. Cooper, X. Dong, C. Bock, E.E. Bouhassira, Y. Fan, High-Resolution Mapping of H1 Linker Histone Variants in Embryonic Stem Cells, PLoS Genet. 9 (2013) e1003417. https://doi.org/10.1371/journal.pgen.1003417.
[16] A. Roque, The preferential binding of histone H1 to DNA scaffold-associated regions is determined by its C-terminal domain, Nucleic Acids Research. 32 (2004) 6111–6119. https://doi.org/10.1093/nar/gkh945.
[17] J.M. Buckwalter, D. Norouzi, A. Harutyunyan, V.B. Zhurkin, S.A. Grigoryev, Regulation of chromatin folding by conformational variations of nucleosome linker DNA, Nucleic Acids Research. 45 (2017) 9372–9387. https://doi.org/10.1093/nar/gkx562.
[18] F. Cui, V.B. Zhurkin, Distinctive sequence patterns in metazoan and yeast nucleosomes: Implications for linker histone binding to AT-rich and methylated DNA, Nucleic Acids Research. 37 (2009) 2818–2829. https://doi.org/10.1093/nar/gkp113.
[19] R. Tomaszewski, The AT-rich flanks of the oocyte-type 5S RNA gene of Xenopus laevis act as a strong local signal for histone H1-mediated chromatin reorganization in vitro, Nucleic Acids Research. 25 (1997) 458–466. https://doi.org/10.1093/nar/25.3.458.
[20] M.A. Ozturk, G.V. Pachov, R.C. Wade, V. Cojocaru, Conformational selection and dynamic adaptation upon linker histone binding to the nucleosome., Nucleic Acids Res. 44 (2016) 6599–6613. https://doi.org/10.1093/nar/gkw514.
[21] G.V. Pachov, R.R. Gabdoulline, R.C. Wade, On the structure and dynamics of the complex of the nucleosome and the linker histone, Nucleic Acids Research. 39 (2011) 5255–5263. https://doi.org/10.1093/nar/gkr101.
[22] M. De, M.A. Öztürk, S. Isbaner, K. Tóth, R.C. Wade, DNA sequence-dependent positioning of the linker histone in a nucleosome: a single-pair FRET study, Biophysical Journal. 0 (2021). https://doi.org/10.1016/j.bpj.2021.07.012.
[23] T.E. Haran, U. Mohanty, The unique structure of A-tracts and intrinsic DNA bending, Quart. Rev. Biophys. 42 (2009) 41–81. https://doi.org/10.1017/S0033583509004752.
[24] P.T. Lowary, J. Widom, New DNA sequence rules for high affinity binding to histone octamer and sequence-directed nucleosome positioning, Journal of Molecular Biology. 276 (1998) 19–42. https://doi.org/10.1006/jmbi.1997.1494.
[25] C. Engler, R. Kandzia, S. Marillonnet, A One Pot, One Step, Precision Cloning Method with High Throughput Capability, PLoS One. 3 (2008) e3647. https://doi.org/10.1371/journal.pone.0003647.
[26] C. Engler, R. Gruetzner, R. Kandzia, S. Marillonnet, Golden Gate Shuffling: A One-Pot DNA Shuffling Method Based on Type IIs Restriction Enzymes, PLoS One. 4 (2009) e5553. https://doi.org/10.1371/journal.pone.0005553.
[27] C. Engler, S. Marillonnet, Golden Gate Cloning, in: S. Valla, R. Lale (Eds.), DNA Cloning and Assembly Methods, Humana Press, Totowa, NJ, 2014: pp. 119–131. https://doi.org/10.1007/978-1-62703-764-8_9.
[28] M. Würtz, D. Aumiller, L. Gundelwein, P. Jung, C. Schütz, K. Lehmann, K. Tóth, K. Rohr, DNA accessibility of chromatosomes quantified by automated image analysis of AFM data, Sci Rep. 9 (2019) 12788. https://doi.org/10.1038/s41598-019-49163-4.

[29] A. Gansen, K. Tóth, N. Schwarz, J. Langowski, Structural Variability of Nucleosomes Detected by Single-Pair Förster Resonance Energy Transfer: Histone Acetylation, Sequence Variation, and Salt Effects, J. Phys. Chem. B. 113 (2009) 2604–2613. https://doi.org/10.1021/jp7114737.
[30] A. Gansen, K. Tóth, N. Schwarz, J. Langowski, Opposing roles of H3- and H4-acetylation in the regulation of nucleosome structure—a FRET study, Nucleic Acids Research. 43 (2015) 1433–1443. https://doi.org/10.1093/nar/gku1354.
[31] A. Gansen, F. Hauger, K. Tóth, J. Langowski, Single-pair fluorescence resonance energy transfer of nucleosomes in free diffusion: Optimizing stability and resolution of subpopulations, Analytical Biochemistry. 368 (2007) 193–204. https://doi.org/10.1016/j.ab.2007.04.047.
[32] A.N. Kapanidis, T.A. Laurence, N.K. Lee, E. Margeat, X. Kong, S. Weiss, Alternating-laser excitation of single molecules, Acc Chem Res. 38 (2005) 523–533. https://doi.org/10.1021/ar0401348.
[33] N.K. Lee, A.N. Kapanidis, Y. Wang, X. Michalet, J. Mukhopadhyay, R.H. Ebright, S. Weiss, Accurate FRET Measurements within Single Diffusing Biomolecules Using Alternating-Laser Excitation, Biophysical Journal. 88 (2005) 2939–2953. https://doi.org/10.1529/biophysj.104.054114.
[34] E.F. Pettersen, T.D. Goddard, C.C. Huang, G.S. Couch, D.M. Greenblatt, E.C. Meng, T.E. Ferrin, UCSF Chimera—A visualization system for exploratory research and analysis, Journal of Computational Chemistry. 25 (2004) 1605–1612. https://doi.org/10.1002/jcc.20084.
[35] S. Kalinin, T. Peulen, S. Sindbert, P.J. Rothwell, S. Berger, T. Restle, R.S. Goody, H. Gohlke, C.A.M. Seidel, A toolkit and benchmark study for FRET-restrained high-precision structural modeling, Nature Methods. 9 (2012) 1218–1225. https://doi.org/10.1038/nmeth.2222.
[36] S. Sindbert, S. Kalinin, H. Nguyen, A. Kienzler, L. Clima, W. Bannwarth, B. Appel, S. Müller, C.A.M. Seidel, Accurate Distance Determination of Nucleic Acids via Förster Resonance Energy Transfer: Implications of Dye Linker Length and Rigidity, J. Am. Chem. Soc. 133 (2011) 2463–2480. https://doi.org/10.1021/ja105725e.
[37] K. Lehmann, R. Zhang, N. Schwarz, A. Gansen, N. Mücke, J. Langowski, K. Toth, Effects of charge-modifying mutations in histone H2A α3-domain on nucleosome stability assessed by single-pair FRET and MD simulations, Sci Rep. 7 (2017) 13303. https://doi.org/10.1038/s41598-017-13416-x.
[38] W.J.A. Koopmans, A. Brehm, C. Logie, T. Schmidt, J. van Noort, Single-Pair FRET Microscopy Reveals Mononucleosome Dynamics, J Fluoresc. 17 (2007) 785–795. https://doi.org/10.1007/s10895-007-0218-9.
[39] V. Böhm, A.R. Hieb, A.J. Andrews, A. Gansen, A. Rocker, K. Tóth, K. Luger, J. Langowski, Nucleosome accessibility governed by the dimer/tetramer interface, Nucleic Acids Research. 39 (2011) 3093–3102. https://doi.org/10.1093/nar/gkq1279.
[40] K. Lehmann, S. Felekyan, R. Kühnemuth, M. Dimura, K. Tóth, C.A.M. Seidel, J. Langowski, Dynamics of the nucleosomal histone H3 N-terminal tail revealed by high precision single-molecule FRET, Nucleic Acids Research. 48 (2020) 1551–1571. https://doi.org/10.1093/nar/gkz1186.
[41] A. Gansen, S. Felekyan, R. Kühnemuth, K. Lehmann, K. Tóth, C.A.M. Seidel, J. Langowski, High precision FRET studies reveal reversible transitions in nucleosomes between microseconds and minutes, Nat Commun. 9 (2018) 4628. https://doi.org/10.1038/s41467-018-06758-1.

[42] K. Suhre, Y.-H. Sanejouand, ElNemo: a normal mode web server for protein movement analysis and the generation of templates for molecular replacement, Nucleic Acids Research. 32 (2004) W610–W614. https://doi.org/10.1093/nar/gkh368.
[43] B. Hellenkamp, S. Schmid, O. Doroshenko, O. Opanasyuk, R. Kühnemuth, S. Rezaei Adariani, B. Ambrose, M. Aznauryan, A. Barth, V. Birkedal, M.E. Bowen, H. Chen, T. Cordes, T. Eilert, C. Fijen, C. Gebhardt, M. Götz, G. Gouridis, E. Gratton, T. Ha, P. Hao, C.A. Hanke, A. Hartmann, J. Hendrix, L.L. Hildebrandt, V. Hirschfeld, J. Hohlbein, B. Hua, C.G. Hübner, E. Kallis, A.N. Kapanidis, J.-Y. Kim, G. Krainer, D.C. Lamb, N.K. Lee, E.A. Lemke, B. Levesque, M. Levitus, J.J. McCann, N. Naredi-Rainer, D. Nettels, T. Ngo, R. Qiu, N.C. Robb, C. Röcker, H. Sanabria, M. Schlierf, T. Schröder, B. Schuler, H. Seidel, L. Streit, J. Thurn, P. Tinnefeld, S. Tyagi, N. Vandenberk, A.M. Vera, K.R. Weninger, B. Wünsch, I.S. Yanez-Orozco, J. Michaelis, C.A.M. Seidel, T.D. Craggs, T. Hugel, Precision and accuracy of single-molecule FRET measurements—a multi-laboratory benchmark study, Nat Methods. 15 (2018) 669–676. https://doi.org/10.1038/s41592-018-0085-0.
[44] T. Schalch, S. Duda, D.F. Sargent, T.J. Richmond, X-ray structure of a tetranucleosome and its implications for the chromatin fibre, Nature. 436 (2005) 138–141. https://doi.org/10.1038/nature03686.
[45] C. Wu, A. Travers, Modelling and DNA topology of compact 2-start and 1-start chromatin fibres, Nucleic Acids Research. 47 (2019) 9902–9924. https://doi.org/10.1093/nar/gkz495.
[46] I. Garcia-Saez, H. Menoni, R. Boopathi, M.S. Shukla, L. Soueidan, M. Noirclerc-Savoye, A. Le Roy, D.A. Skoufias, J. Bednar, A. Hamiche, D. Angelov, C. Petosa, S. Dimitrov, Structure of an H1-Bound 6-Nucleosome Array Reveals an Untwisted Two-Start Chromatin Fiber Conformation, Molecular Cell. 72 (2018) 902-915.e7. https://doi.org/10.1016/j.molcel.2018.09.027.
[47] W. Alvarado, J. Moller, A.L. Ferguson, J.J. de Pablo, Tetranucleosome Interactions Drive Chromatin Folding, ACS Cent. Sci. 7 (2021) 1019–1027. https://doi.org/10.1021/acscentsci.1c00085.
[48] Y. Takizawa, C.-H. Ho, H. Tachiwana, H. Matsunami, W. Kobayashi, M. Suzuki, Y. Arimura, T. Hori, T. Fukagawa, M.D. Ohi, M. Wolf, H. Kurumizaka, Cryo-EM Structures of Centromeric Tri-nucleosomes Containing a Central CENP-A Nucleosome, Structure. 28 (2020) 44-53.e4. https://doi.org/10.1016/j.str.2019.10.016.
[49] D.C. Woods, J. Wereszczynski, Elucidating the influence of linker histone variants on chromatosome dynamics and energetics, Nucleic Acids Research. 48 (2020) 3591–3604. https://doi.org/10.1093/nar/gkaa121.